"Free" Volume Expansion and Formation Enthalpy of Defects as Key Parameters Tuning the Oxide Ionic Conductivity in Derivatives of β-La2Mo2O9

Gwenaël Corbel, Ania Selmi, Emmanuelle Suard, Philippe Lacorre

"Free" Volume Expansion and Formation Enthalpy of Defects as Key Parameters Tuning the Oxide Ionic Conductivity in Derivatives of β-$La_2Mo_2O_9$

Gwenaël CORBEL [1*], Ania SELMI [1], Emmanuelle SUARD [2] and Philippe LACORRE [1]

[1] LUNAM, Université du Maine,
Institut des Molécules et Matériaux du Mans, UMR-6283 CNRS,
Avenue Olivier Messiaen, 72085 Le Mans Cedex 9, France

[2] Institut Laue-Langevin, BP 156, 38042 Grenoble Cedex 9, France

ABSTRACT: The crystal structure of fast oxide-ion conductor β-$La_{1.85}Ba_{0.15}Mo_2O_{8.925}$ and its thermal evolution have been studied using neutron powder diffraction, and compared to those already published [G. Corbel et al., *Chem. Mater.* **2011**, *23*, 1288] of a bismuth counterpart in the LAMOX family, β-$La_{1.7}Bi_{0.3}Mo_2O_9$. Comparable evolutions have a tendency to suggest that the observed behavior, a specific combination of rotation and distortion of cationic building units, is a common feature of La-substituted β-LAMOX compounds. For the first time in crystallized solids, a quantitative link is made for both compounds between the high-temperature (high-T) conductivity increase relative to Arrhenius behavior and the volume expansion of the voids, through consecutive fits to crystallographic and conductivity data of the Dienes–Macedo–Litovitz (DML) equation. Both the expansion of the "free" volume (V_F) and the formation enthalpy of the Frenkel defects (ΔH_f) are the key parameters tuning the conductivity of LAMOX compounds above T_0 = 400–450 °C. A substitution strategy of La in $La_2Mo_2O_9$ is proposed in order to optimize anionic conductivity, based on crystallographic grounds.

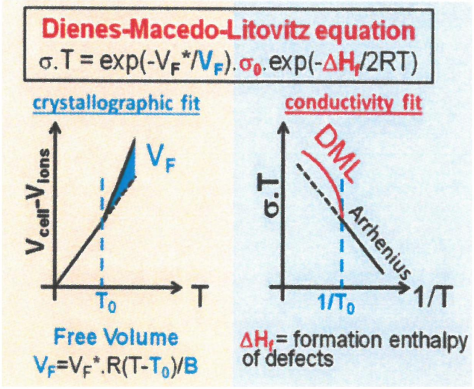

INTRODUCTION

Fast oxide ion conductors are of considerable interest for "clean" electrochemical applications, including solid oxide fuel cells, oxygen sensors, and oxygen separation membranes. In this field, Lacorre et al. discovered a novel oxide ion conductor 14 years ago: $La_2Mo_2O_9$.[1,2] This binary oxide exhibits, above a first-order and reversible α (monoclinic, $P2_1$) to β (cubic, $P2_13$) structural phase transition at 580 °C, an anionic conductivity (5×10^{-2} S cm^{-1} at 700 °C) higher than that of the conventional 8 mol % yttria-stabilized zirconia SOFC electrolyte[3] (see Figure 1). Therefore, the strategy was to stabilize the high-temperature (high-T) anionically disordered cubic β-form through solid-solution formation in order to enhance the oxide ion conductivity at lower temperatures. Numerous possible substitutions such as $(La_{2-x}A^{n+}{}_x)Mo_2O_{9-(3-n)x/2}$ (A^+ = Na,[4] K,[4–7] Rb;[4] A^{2+} = Ca, Sr, Ba, Pb;[6–8] A^{3+} = Bi,[9] Pr,[10] Nd,[11,12] Eu,[13,14] Gd,[15] Y[15]), $La_2Mo_{2-y}B^{n+}{}_yO_{9-(6-n)y/2}$ (B^{5+} = V,[16] Nb,[17,18] Ta;[18] B^{6+} = S,[19] Cr,[20] W[20,21]) and $La_2Mo_2O_{(9-0.5y)}F_y$[22] have been reported. Apart from Na^+, Pr^{3+}, Nb^{5+} and F^-, most substitutes for La or Mo in $La_2Mo_2O_9$ stabilize, above certain contents, the cubic β-form at room temperature.

These chemically β-stabilized LAMOX compounds exhibit, with a higher or lower magnitude, depending on the nature (isovalent/aliovalent with or without a lone pair) and the amount of substitute, a concomitant increase of the thermal expansion coefficient and of the conductivity above 400–450 °C.[13] Above 450 °C, the thermal evolution of the conductivity can be satisfactorily fitted by a Vogel–Tammann–Fulcher (VTF) model,[23–25] thus suggesting a regime of framework-assisted mobility of oxide ions. A thorough temperature-controlled powder neutron diffraction study was carried out on a Bi-substituted LAMOX oxide ion conductor, β-$La_{1.7}Bi_{0.3}Mo_2O_9$,[26] in order to identify the subtle structural distortions at the origin of, or correlated to, the peculiarities of the ionic conduction process. This investigation revealed that the main distortions concern the geometry of the antitetrahedral $[O1(La,Bi)_3Mo]$ building units of the cationic framework hosting conducting anions, rather than the tilt/rotation of such units, as previously postulated.[27] An analysis of the ionic displacements within these $[O1(La,Bi)_3Mo]$ units upon heating suggests that the successive expansions of $[(La,Bi)_3]$ and $[(La,Bi)_2Mo]$ triangular faces enables some O1 oxide ions to escape from their initial position toward partially occupied O2 and O3 sites, respectively. The increase of ionic conductivity/mobility observed above ca. 450 °C in β-$La_{1.7}Bi_{0.3}Mo_2O_9$ and ascribed to a transition toward a VTF-type assisted transport regime would consequently be due to the opening up of new conduction paths, rather than to an intrinsic increase in

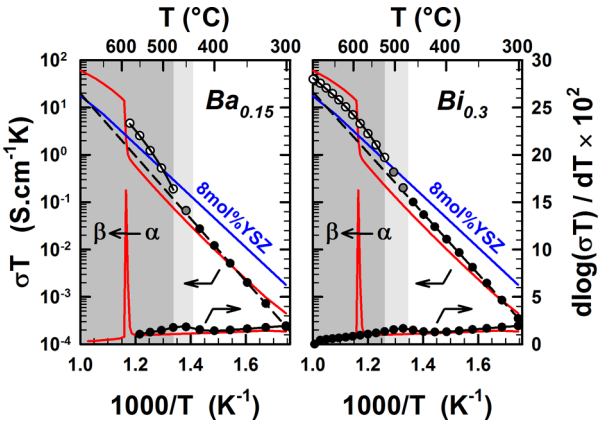

Figure 1. Temperature dependence of the electrical conductivity of β-$La_{1.7}Bi_{0.3}Mo_2O_9$ (black, gray, and open circles) and of β-$La_{1.85}Ba_{0.15}Mo_2O_{8.925}$ (black, gray, and open circles) compared to that of $La_2Mo_2O_9$ (pellet sintered for 3 h at 1000 °C, relative density = 96(1)% of theoretical density, solid red line) and to that of 8 mol % yttria-stabilized zirconia (solid blue line, data taken from ref 3). The conductivity plot was fitted with a conventional Arrhenius law in the linear part at low temperature (dashed black line) and with the DML model when departure from linearity is observed at higher temperature (solid black line). Gray circles refer to a mixed Arrhenius–DML regime. At the bottom, a plot of the first derivative of the conduction, with respect to temperature, is shown (black circles).

mobility of O2 and O3 ions on their low-temperature conduction paths.

In 1959, Cohen and Turnbull[28] proposed a microscopic interpretation of the VTF equation modeling the molecular transport in liquids:

$$\phi T = A \exp\left[- \frac{B}{R(T - T_0)} \right]$$

where ϕ is the fluidity. These authors postulated that a molecule vibrates about an equilibrium position until a redistribution of local "free" volumes opens up, in its vicinity, a void of sufficient size to jump into, thus facilitating its diffusion in the liquid. They showed that two parameters of this empirical VTF relation (B and T_0) are directly linked to the thermal expansion of the total "free" or empty volume available in the liquid for the diffusion of molecules. If a "free volume"-type mechanism drives the oxide anion migration above 400–450 °C in the chemically β-stabilized LAMOX compounds, it implies that the distortions of the $[La_3Mo]$ antitetrahedra-based framework taking place above this temperature release a "free" volume. According to the Cohen and Turnbull interpretation, this "free" volume must expand as the distortions increase upon heating, to explain the singular increase of the conductivity observed. A rational fine-tuning of the "free" volume expansion is highly desirable to enhance the oxide ionic conductivity but is also challenging. Bearing in mind that the cationic framework of the β-$La_2Mo_2O_9$ structure is composed of La corner-sharing $[O1La_3Mo]$ antitetrahedra, increasing the average size of the bridging ion could open the way to increase the total "free" volume through the expansion in volume of both the antitetrahedron, the cages and the tunnels of the antistructure. Among all possible substitutes for lanthanum, only potassium (ionic radius in 10-fold coordination of 1.59 Å[29]), barium (ionic radius in 10-fold coordination of 1.52 Å[29]), or divalent lead (ionic radius in 10-fold coordination of 1.40 Å[29]) can increase, even at low substitution rate, the mean La site cation radius $\langle r \rangle$ more than Bi does in β-$La_{1.7}Bi_{0.3}Mo_2O_9$ ($\langle r \rangle$ = 1.276 Å with an ionic radius for La^{3+} and Bi^{3+} in 10-fold coordination of 1.27 and 1.31 Å, respectively[29]). Such partial substitutions of La by an element of lower valence change the oxide ion/vacancy balance. One can consider that both the increase of the mean La-site cation radius and the introduction of extrinsic oxygen vacancies could enhance the oxide ion migration. However, the reverse situation is observed in all aliovalently substituted LAMOX compounds reported in the literature. As shown by Marrero-López et al.[6] or very recently by Takai et al.,[8] the ionic conductivity of K-, Ba-, and Pb-substituted compounds remains lower than that measured at temperatures higher than 580 °C in the parent compound β-$La_2Mo_2O_9$. Whatever the substitute considered, the conductivity decreases nonlinearly as the substitution rate increases.

Our previous investigations[7] showed that the β-form of the highest K^+- and Ba^{2+}-substituted LAMOX exhibit an exsolution of β-$KLaMo_2O_8$ and $BaMoO_4$ scheelite-type phases above a temperature decreasing as the substitute content increases: $La_{1.92}K_{0.08}Mo_2O_{8.92}$ (~700 °C), $La_{1.88}K_{0.12}Mo_2O_{8.88}$ (~500 °C), $La_{1.85}Ba_{0.15}Mo_2O_{8.925}$ (~900–950 °C), and $La_{1.8}Ba_{0.2}Mo_2O_{8.9}$ (~700 °C). In this series, β-$La_{1.85}Ba_{0.15}Mo_2O_{8.925}$ is the only composition combining both the "highest" mean La-site cation radius ($\langle r \rangle$ = 1.289 Å) and a stability of the β-form in a temperature range (up to 900 °C) as large as the range explored in our previous structural analysis performed on β-$La_{1.7}Bi_{0.3}Mo_2O_9$ derivative, thus allowing a direct comparison. The objective of the current structural analysis on β-$La_{1.85}Ba_{0.15}Mo_2O_{8.925}$, undertaken by temperature-controlled neutron diffraction, was to understand why no enhancement of the ionic conductivity can be achieved through a concomitant increase of the mean La-site ionic radius and the introduction of extrinsic vacancies. In the first part of the paper, the temperature incidence on the geometry and tilts/rotations of $[O1La_3Mo]$ elementary building units in β-$La_{1.85}Ba_{0.15}Mo_2O_{8.925}$ is at first carefully examined and then compared with the one previously determined in β-$La_{1.7}Bi_{0.3}Mo_2O_9$ to highlight the structural changes caused by barium. As shown in the current paper, the oxide ion conductivity of β-$La_{1.85}Ba_{0.15}Mo_2O_{8.925}$ and β-$La_{1.7}Bi_{0.3}Mo_2O_9$ at temperatures higher than 425 °C are similar, although the volume of the voids expands as the mean La-site ionic radius increases. This contradiction led us to reconsider the use of the VTF equation to describe the temperature dependence of the conductivity of LAMOX materials. Finally, we show how well the modification of the VTF equation proposed by Dienes,[30] and Macedo and Litovitz,[31] can relate the structural features of LAMOX materials to their transport property. A lanthanum substitution strategy based on crystallographic grounds is then proposed for enhancing the oxide ion conductivity of chemically β-stabilized $La_2Mo_2O_9$ compounds above 400–450 °C.

EXPERIMENTAL SECTION

Synthesis. One gram of polycrystalline sample of β-$La_{1.85}Ba_{0.15}Mo_2O_{8.925}$ was prepared by conventional solid-state reaction from elementary oxides La_2O_3 (REacton, 99.9%, from Alfa Aesar), $BaCO_3$ (RP Normapur, 99.5%, from Prolabo), and MoO_3 (PURATREM 99.999% from Strem Chemicals). Prior to use, $BaCO_3$ was kept dry in an air oven at 100 °C and La_2O_3 was calcined in air for 12 h at 1000 °C in order to remove adsorbed water and carbon dioxide (CO_2). Reactant powders were stoichiometrically weighed, thoroughly ground in an agate mortar, and initially heated in

an alumina crucible at 500 °C for 12 h. After several intermediate heatings and regrindings, a single β-phase was finally obtained after a final firing at 1000 °C, followed by cooling to room temperature at a rate of 5 °C/min. Phase purity was checked by recording powder X-ray diffraction patterns at room temperature on a PANalytical θ/θ Bragg–Brentano X'pert MPD PRO diffractometer (Cu $K\alpha_{1+2}$ radiations) equipped with the X'Celerator multielement detector. The above process was performed 10 times to get the 10 g of β-$La_{1.85}Ba_{0.15}Mo_2O_{8.925}$ sample used in the neutron diffraction study.

Structural Characterization. A constant-wavelength (1.593641 Å) neutron powder diffractogram was recorded in static air from the high-resolution two-axis diffractometer super-D2B of Institut Laue–Langevin (Grenoble, France) equipped with a standard ILL furnace. For data collection at and above room temperature, the 10-g sample of β-$La_{1.85}Ba_{0.15}Mo_2O_{8.925}$ was loaded in a cylindrical silica glass container open to air in order to avoid the molybdenum reduction upon heating. Temperature-controlled neutron diffractograms were collected at RT and then at 100 °C intervals between 100 and 900 °C. Data were collected in the [−7.45°−162°] scattering angle range for approximately 2 h at each temperature with a 0.05° step. The program FullProf[32] was used for Rietveld refinements. The lineshape was modeled by a standard pseudo-Voigt function using a Caglioti full width at half maximum (fwhm)-type function (refined parameters U, V, W, η) with a profile asymmetry correction (reported by Bérar and Baldinozzi[33]) below a scattering angle of 40° in 2θ (two first adjustable parameters). In addition to the modulated background arising from short-range correlation of atomic positions O2 and O3 with fractional occupancies in β-$La_2Mo_2O_9$-type structure,[20,26,34,35] all neutron diffraction patterns collected in a cylindrical vitreous silica container in the temperature range from RT to 900 °C and shown in Figure 2 exhibit three parasitic broad peaks of the vitreous silica container at Q-wave vector positions of 1.5, 2.9, and 5.5 Å^{-1}.[36] Then, the wavy background intensity was estimated from linear interpolation between points manually selected in regions free from Bragg reflections of space group $P2_13$ (No. 198). The Diamond software[37] was used to draw the crystal structure.

Transport Property. A dense ceramic sample of β-$La_{1.85}Ba_{0.15}Mo_2O_{8.925}$ was obtained after cold pressing the ball-milled powder and sintering the pellet at 1000 °C (relative density = 94(2)% of theoretical density), as extensively described in ref 13. Thin Pt films electrodes were deposited by radio-frequency (RF) sputtering on both flat faces of the sintered pellet. Conductivity was measured by using a symmetric two-electrodes electrochemical cell connected to a Solartron 1296 dielectric interface and a Solartron 1260 frequency response analyzer. Complex impedance spectra were recorded over the 10 MHz to 0.05 Hz range (AC signal amplitude of 50 mV, 40 points/decade) under dry air flow every 25 °C (thermal equilibration for 35 min) as the temperature increased from 300 °C to 575 °C. As previously stated in β-$La_{1.9}Ba_{0.1}Mo_2O_{8.95}$,[7] a decrease in conductivity resulting from the exsolution of $BaMoO_4$ within the pellet takes place above 600–650 °C, while the raw powder remains pure up to 900–950 °C. Thereby, no conductivity measurements on β-$La_{1.85}Ba_{0.15}Mo_2O_{8.925}$ were performed at temperatures higher than 575 °C.

RESULTS AND DISCUSSION

Rietveld Refinements. The crystal structure of β-$La_{1.85}Ba_{0.15}Mo_2O_{8.925}$, at room temperature, has been refined from neutron powder diffraction pattern by the Rietveld method using the high-temperature cubic structure of β-$La_2Mo_2O_9$ as a starting structural model.[15] The site occupation factors for La and Ba in special positions (4a) were kept fixed to 0.925 and 0.075, respectively, according to nominal Ba content. In our first structural model (model 1), it was postulated that the extrinsic oxygen vacancies introduced by the aliovalent substitution of lanthanum by barium were located on O2/O3 sites, since no deficiency of the O1 site was earlier reported in β-$La_2Mo_2O_9$ or β-$La_{1.7}Bi_{0.3}Mo_2O_9$.[26] Thereby, the occupancy of

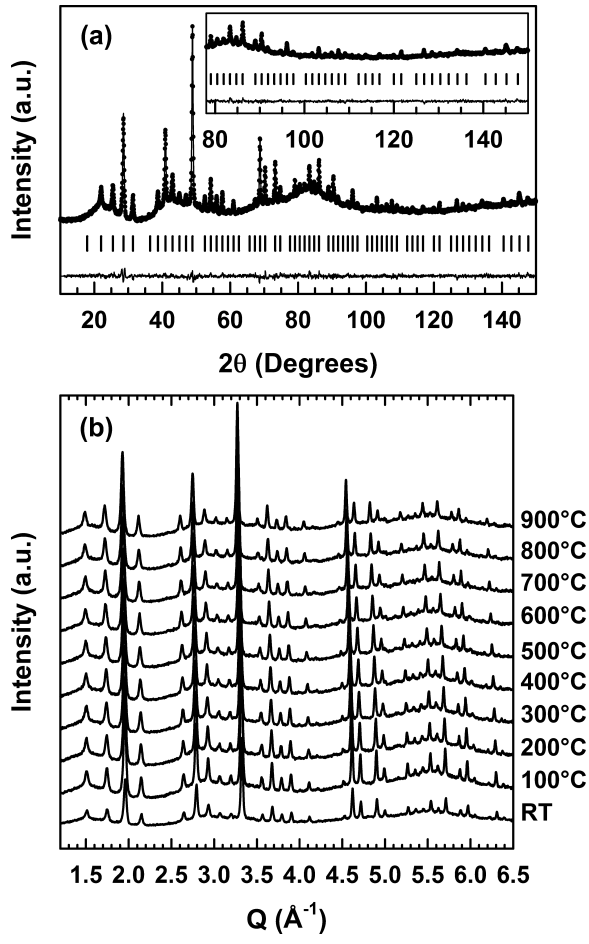

Figure 2. Neutron diffraction patterns of β-$La_{1.85}Ba_{0.15}Mo_2O_{8.925}$: (a) observed (dots), calculated (lines), and difference (below) patterns at room temperature (RT) using the structural model in Table 1. Vertical markers give Bragg peak positions of space group $P2_13$ (No. 198). (b) Modulation of the background showing a first maximum around a Q-wave vector position of 2.75 Å^{-1} ($Q = 4\pi \sin\theta/\lambda$) and the parasitic broad peaks of vitreous silica container at 1.5, 2.9, and 5.5 Å^{-1} for patterns collected from RT to 900 °C (see text for details).

the O3 site was initially constrained with that of the O2 site to fulfill oxygen stoichiometry "$O_{8.925}$". The anisotropic temperature factors U_{ij} of O3 site were also constrained to those of O2. The neutron diffraction pattern collected at room temperature was satisfactorily modeled by least-squares fitting the structural model, which consisted of 10 atomic coordinates, 12 anisotropic thermal factors, O2/O3 fractional site occupancies, and the cubic cell parameter a. Figure 2a shows the final observed, calculated, and difference diffraction patterns of β-$La_{1.85}Ba_{0.15}Mo_2O_{8.925}$ at room temperature. In Figure 2b, no trace of exsolved $BaMoO_4$ is detected in the neutron diffraction patterns collected in the temperature range of 100–900 °C. It confirms that raw powder of β-$La_{1.85}Ba_{0.15}Mo_2O_{8.925}$ is stable in air up to 900 °C and that the exsolution takes place at temperatures higher than 900 °C. Then, successively, the structure refined at a lower temperature was used as starting model for refinement of the next-higher-temperature one. All neutron diffraction patterns were satisfactorily modeled by least-squares fitting this structural model. The values of atomic parameters (positions coordinates, equivalent isotropic temperature factors,[38] and site occupancy factors) together with

Table 1. Results of Rietveld Refinement for β-$La_{1.85}Ba_{0.15}Mo_2O_{8.925}$ (Cubic Space Group $P2_13$, No. 198) from Neutron Powder Diffraction Data[a]

parameter	RT	100 °C	200 °C	300 °C	400 °C	500 °C	600 °C	700 °C	800 °C	900 °C
a (Å)	7.1809(1)	7.1879(2)	7.1972(2)	7.2089(2)	7.2201(2)	7.2345(2)	7.2500(2)	7.2644(2)	7.2782(2)	7.2919(2)
V (Å^3)	370.29(1)	371.37(2)	372.81(2)	374.63(2)	376.38(2)	378.64(2)	381.08(2)	383.35(2)	385.54(2)	387.72(2)

atom	multiplicity and Wyckoff letter	positions coordinates	RT	100 °C	200 °C	300 °C	400 °C	500 °C	600 °C	700 °C	800 °C	900 °C
La/Ba	4a	x	0.8538(3)	0.8531(3)	0.8543(3)	0.8534(3)	0.8536(3)	0.8524(3)	0.8512(4)	0.8509(4)	0.8507(4)	0.8504(4)
		B_{eq} (Å^2)[b]	4.3(1)	4.8(1)	4.5(1)	4.7(1)	4.6(1)	5.2(1)	5.3(1)	5.9(2)	5.2(1)	6.0(2)
		occupancy	0.925/0.075	0.925/0.075	0.925/0.075	0.925/0.075	0.925/0.075	0.925/0.075	0.925/0.075	0.925/0.075	0.925/0.075	0.925/0.075
Mo	4a	x	0.1681(6)	0.1679(6)	0.1687(6)	0.1694(6)	0.1702(5)	0.1693(6)	0.1700(6)	0.1678(7)	0.1681(7)	0.1685(7)
		B_{eq} (Å^2)[b]	3.58(8)	3.67(6)	3.78(7)	3.93(7)	3.78(7)	3.90(7)	4.06(7)	4.11(7)	4.47(9)	4.65(9)
		occupancy	1	1	1	1	1	1	1	1	1	1
O1	4a	x	0.3139(7)	0.3137(7)	0.3150(7)	0.3171(7)	0.3179(7)	0.3188(6)	0.3193(6)	0.3171(7)	0.3169(8)	0.3185(8)
		B_{eq} (Å^2)[b]	5.6(2)	5.9(2)	7.1(2)	7.7(2)	7.4(2)	7.0(2)	7.0(2)	7.5(2)	7.8(2)	8.9(3)
		occupancy	1	1	1	1	1	1	1	1	1	1
O2	12b	x	0.9908(6)	0.9907(5)	0.9892(5)	0.9880(6)	0.9857(6)	0.9867(6)	0.9863(7)	0.9857(8)	0.9853(7)	0.9851(8)
		y	0.180(1)	0.180(1)	0.178(1)	0.176(1)	0.175(1)	0.174(1)	0.170(1)	0.174(1)	0.172(1)	0.172(2)
		z	0.345(1)	0.343(1)	0.339(1)	0.339(1)	0.335(1)	0.335(1)	0.331(1)	0.333(1)	0.329(2)	0.328(2)
		B_{eq} (Å^2)[b]	7.3(3)	7.3(3)	7.9(3)	8.6(3)	9.0(3)	8.9(3)	9.1(3)	10.4(4)	10.4(5)	11.3(5)
		occupancy	0.837(6)	0.834(6)	0.840(6)	0.841(6)	0.852(7)	0.848(7)	0.855(7)	0.872(8)	0.866(10)	0.862(11)
O3	12b	x	0.915(1)	0.917(1)	0.913(1)	0.911(2)	0.916(2)	0.920(2)	0.925(2)	0.921(2)	0.925(3)	0.923(3)
		y	0.626(2)	0.624(2)	0.621(2)	0.615(3)	0.611(3)	0.615(3)	0.605(3)	0.605(4)	0.604(4)	0.611(5)
		z	0.559(1)	0.558(1)	0.556(1)	0.553(1)	0.550(2)	0.553(2)	0.554(2)	0.549(2)	0.550(3)	0.546(3)
		B_{eq} (Å^2)[b]	7.3(3)	7.3(3)	7.9(3)	8.6(3)	9.0(3)	8.9(3)	9.1(3)	10.4(4)	10.4(5)	11.3(5)
		occupancy	0.317(6)	0.320(6)	0.314(6)	0.313(6)	0.302(7)	0.306(7)	0.299(7)	0.282(8)	0.288(10)	0.292(11)
no. of reflections			152	154	154	154	154	154	154	154	156	156
R_{wp} (%)			16.1	14.9	15.0	15.1	15.1	15.0	14.8	15.3	15.2	15.4
R_{exp} (%)			23.23	17.38	17.44	17.85	18.05	18.30	18.50	18.79	19.39	19.90
χ^2			0.479	0.731	0.743	0.720	0.696	0.668	0.638	0.664	0.618	0.602
R_{Bragg} (%)			7.72	9.09	9.22	8.58	9.81	9.04	8.97	10.0	8.81	9.51

[a]For each temperature, lattice parameters, positions coordinates, equivalent isotropic temperature factors, and site occupancy factors are listed, as well as R-factors and χ^2 values for the fit. [b]$B_{eq} = (4a^2/3)[\beta_{11} + \beta_{22} + \beta_{33}]$.

Table 2. Sintering Conditions, Relative Density, and Parameters of the Arrhenius and the Dienes−Macedo−Litovitz (DML)[30,31]-Type Laws Determined for β-$La_{1.7}Bi_{0.3}Mo_2O_9$ and β-$La_{1.85}Ba_{0.15}Mo_2O_{8.925}$

	β-$La_{1.7}Bi_{0.3}Mo_2O_9$	β-$La_{1.85}Ba_{0.15}Mo_2O_{8.925}$
sintering conditions	5 h, 875 °C	12 h, 1000 °C
relative density (%)	98(1)	94(2)
Arrhenius regime, $\sigma T = \sigma_0 \exp\left(-\frac{E_a}{RT}\right)$		
$\log(\sigma_0)$ (S K cm^{-1})	7.74	7.90
E_a (eV)	1.27	1.31
r^2	0.9999	0.9999
DML regime, $\sigma T = \sigma_0 \exp\left(-\frac{\Delta H_f}{2RT}\right) \exp\left[-\frac{B}{R(T-T_0)}\right]$		
$\log(\sigma_0)$ (S K cm^{-1})	4.99	6.37
ΔH_f (eV)	1.10	1.68
B (eV)	0.037	0.028
T_0 (°C)	402	376
r^2	0.999	0.999
migration enthalpy ΔH_m[a] (eV)	0.72	0.47

[a] $E_a = \Delta H_f/2 + \Delta H_m$.

conventional reliability factors, are reported in Table 1 for each temperature of the data collection.

At this stage, one can wonder whether the presence of extrinsic oxygen vacancies in the anionic sublattice of β-$La_{1.85}Ba_{0.15}Mo_2O_{8.925}$ could have changed the overall oxygen vacancy (intrinsic+extrinsic) distribution over the three crystallographic oxygen sites of the structure. Therefore, a second structural model (model 2) was tested, in which a slight 5% depletion of the O1 site to the benefit of O2 or O3 sites was introduced. The starting occupancy of each oxygen site was then calculated to fulfill oxygen stoichiometry "$O_{8.925}$". The refinement of the occupancy factors of O1, O2, and O3 sites was performed while keeping all structural parameters fixed to values reported in Table 1. To retain the "$O_{8.925}$" oxygen stoichiometry, occupancies of two oxygen sites were, in turn, constrained and refined. The deficiency of O1 site in β-$La_{1.85}Ba_{0.15}Mo_2O_{8.925}$ was ~0.5(5)% at RT or 900 °C, thus remaining of the same order of magnitude as that the deficiency previously determined for β-$La_{1.7}Bi_{0.3}Mo_2O_9$ (0.2(4)% at 900 °C). The absence of a significant depletion of O1 site implies that the (intrinsic+extrinsic) oxygen vacancies only reside at O2 and O3 sites whatever the temperature. The thorough structural analysis reported hereafter was thereby carried out from the crystallographic data of model 1 (Table 1).

Anionic Conductivity. The incidence of the aliovalent substitution of lanthanum by barium on the conductivity of $La_2Mo_2O_9$ was earlier studied by Marrero-López et al.[6] Their attention was focused on two compositions $x = 0.025$ and 0.15 of the $La_{2-x}Ba_xMo_2O_{9-x/2}$ solid solution. The conductivity measurements were performed up to 950 °C on dense pellets directly prepared from nanocrystalline powders. Our temperature dependence of the bulk conductivity of β-$La_{1.85}Ba_{0.15}Mo_2O_{8.925}$ in the temperature range of 300−575 °C, displayed in Figure 1, is very similar to that found by these authors. However, none of their $x = 0.025$ and $x = 0.15$ compositions exhibit any decrease of conductivity at temperatures higher than 575 °C. This discrepancy suggests that ball-milling of barium-substituted compounds is likely to involve an exsolution of $BaMoO_4$ at a lower temperature than that reported for raw powders. As shown in Figure 1, the temperature dependence of the bulk conductivity of β-$La_{1.85}Ba_{0.15}Mo_2O_{8.925}$ composition in the temperature range of 300−425 °C can be satisfactorily fitted (correlation coefficient of $r^2 = 0.9999$) with a conventional Arrhenius-type law:

$$\sigma T = \sigma_0 \exp\left(-\frac{E_a}{RT}\right)$$

Values of the pre-exponential factor (σ_0) and the activation energy (E_a) are both reported in Table 2. Note that our value of activation energy determined for the $x = 0.15$ compound in the Arrhenius regime is identical to the value obtained by Marrero-López et al.[6] At temperatures higher than 425−450 °C, the singular increase of the conductivity, characteristic of all chemically β-stabilized LAMOX compounds, is also observed for β-$La_{1.85}Ba_{0.15}Mo_2O_{8.925}$. When compared to the conductivity of β-$La_{1.7}Bi_{0.3}Mo_2O_9$ above 425 °C, no enhancement of the ionic conductivity is achieved through the concomitant increase of the mean La-site ionic radius and the introduction of extrinsic oxygen vacancies (see Figure 1).

Nonoccupied Cell Volume and Structural Distortion. As mentioned in the Introduction, by partially substituting trivalent lanthanum (La^{3+}) with larger divalent barium (Ba^{2+}), we expect to expand the voids of the cationic framework, in order to enhance the overall oxide ion mobility. Since the oxide ion conductivities of β-$La_{1.85}Ba_{0.15}Mo_2O_{8.925}$ and β-$La_{1.7}Bi_{0.3}Mo_2O_9$ at temperatures higher than 425 °C are similar, what we want to know now is whether or not the volume of the voids in β-$La_{1.85}Ba_{0.15}Mo_2O_{8.925}$ is higher than that in β-$La_{1.7}Bi_{0.3}Mo_2O_9$.

Brown et al. have demonstrated that, in ionic solids, the magnitude of the bond lengthening when the temperature increases is dependent both on the amplitude of the thermal vibrations of atoms that form the bond and on the bond strength.[39] Thus, the thermal volume expansion or contraction of the unit cell only originates from the lengthening of chemical bonds and the opening or closing of bond angles with increasing temperature, all ionic radii remaining constant. In β-$La_2Mo_2O_9$, taking into account the partial occupancy of O2 and O3 sites, the average number of oxygen atoms surrounding La^{3+} and Mo^{6+} are 10 and 4.5, respectively. The values of the ionic

radii for La^{3+}, Bi^{3+}, and Ba^{2+} in 10-fold coordination tabulated by Shannon[29] have been used to calculate the volume occupied by ions in the unit cell of β-$La_{1.7}Bi_{0.3}Mo_2O_9$ and β-$La_{1.85}Ba_{0.15}Mo_2O_{8.925}$. With the coordination number of the Mo atom being half an integer, an ionic radius for Mo^{6+} of r_{Mo} = 0.455 Å has been calculated, which is the average of ionic radii in four-fold (0.41 Å) and five-fold (0.50 Å) coordinations. At each temperature, the nonoccupied cell volume has been then calculated for both compounds by subtracting the volume occupied by ions from the cubic unit cell volume determined from Rietveld refinements of neutron diffraction patterns (see Table 1 and ref 26). Note that, a distinction must be made between the cell volume not occupied by ions and the "free" cell volume, which is considered to be the volume available for the migration of oxide ions. Figure 3 displays the evolution

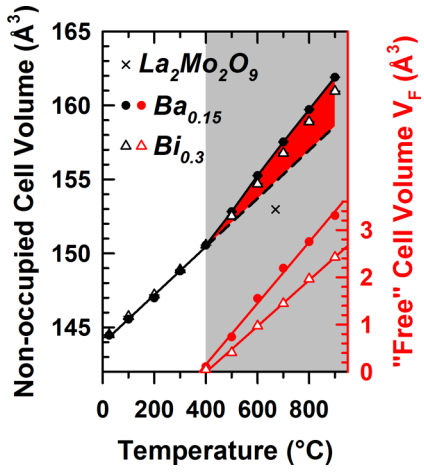

Figure 3. Comparison of temperature dependence of nonoccupied cell volume and of "free" volume for β-$La_{1.85}Ba_{0.15}Mo_2O_{8.925}$ (circles, ●) with that of β-$La_{1.7}Bi_{0.3}Mo_2O_9$ (open triangles, △), both determined from Rietveld refinement of temperature-controlled neutron diffraction data (see Table 1 and ref 26, respectively). Area shown in red corresponds to the "free" volume released by the distortive expansion of the cationic framework taking place above 400 °C in β-$La_{1.85}Ba_{0.15}Mo_2O_{8.925}$ (rotation and distortion of the antitetrahedron). The value of nonoccupied cell volume determined for β-$La_2Mo_2O_9$ at 670 °C (cross symbol, ×) is added for reference (see details in the text).

against temperature of the nonoccupied cell volume for both compounds. It is worth mentioning that the spatial extension of the Bi $6s^2$ lone pair in β-$La_{1.7}Bi_{0.3}Mo_2O_9$ (which roughly corresponds to the volume of an oxide anion[40]) was not considered into the calculation, since no significant distortion of the oxide coordination environment for La/Bi cation site, characteristic of a high stereochemical activity of the lone pair, was noticed in our previous structural analysis.[26]

In Figure 3, two thermal domains with linear dependences of the nonoccupied cell volume are noticed below and above 400 °C. The thermal volume expansion coefficient (TVEC, calculated from the slope and the intercept of the linear regression) increases from 11.3 × 10^{-4} $°C^{-1}$ to 16.1 × 10^{-4} $°C^{-1}$ in the temperature range from 25−400 °C to 400−900 °C, respectively. It must be noted that the TVEC value at high temperature for β-$La_{1.85}Ba_{0.15}Mo_2O_{8.925}$ is higher than the value determined in the same temperature range for β-$La_{1.7}Bi_{0.3}Mo_2O_9$ (11.2 × 10^{-4} $°C^{-1}$ and 14.7 × 10^{-4} $°C^{-1}$ in the ranges of 25−400 °C and 400−900 °C, respectively) whereas both compounds exhibit a similar expansion in nonoccupied cell volume at low temperature. In Figure 3, a difference in nonoccupied cell volume of ∼0.94 Å^3 (∼0.17%) is noted at 900 °C between the two derivatives of $La_2Mo_2O_9$. Comparing the nonoccupied volume releases in the unit cell by the introduction of extrinsic vacancies (approximately +1.58 Å^3 = 0.15 × $^4/_3$ × π × r_V^3, where the ionic radius (r_V) of an oxygen vacancy corresponds to the ionic radius in triangular coordination r_O = 1.36 Å[29] of the oxide ions O(2)/O(3) in β-$La_2Mo_2O_9$[41]) with the increase of the volume occupied by cations in the unit cell (∼+1.34 Å^3) due to the change in the nature and the amount of substitute ($La_{1.7}Bi_{0.3}$ → $La_{1.85}Ba_{0.15}$), the gain in nonoccupied volume represents only one-fourth (∼0.24 Å^3) of the difference in the entire nonoccupied cell volume (∼0.94 Å^3) noted at 900 °C between Bi- and Ba-substituted LAMOX compounds. In other words, the main increase in nonoccupied cell volume of ∼+0.7 Å^3 at 900 °C (which also corresponds to the increase in unit-cell volume) originates from the structural distortion caused by the introduction of barium in the cationic framework. In order to determine these structural changes, the temperature incidence on the structural distortion of the [O1(La/Ba)Mo] host framework in β-$La_{1.85}Ba_{0.15}Mo_2O_{8.925}$ has been carefully examined and compared with that reported for β-$La_{1.7}Bi_{0.3}Mo_2O_9$. The next section is devoted to such analysis.

Distortive Expansion of the [O1(La/Ba)Mo] Host Framework upon Heating. In our previous thorough structural analysis carried out on β-$La_{1.7}Bi_{0.3}Mo_2O_9$, the tunnels of the antistructure, hosting partially occupied O2 and O3 crystallographic sites, have been described as resulting from the 3D interconnections of small cages built up from seven La/Bi corner-sharing [O1(La/Bi)$_3$Mo] basic units. A complete description of the cage geometry has been proposed, using the following parameters:

- six intertetrahedral edge angles between adjacent La corner-sharing [O1La$_3$Mo] basic units: α = La1−La2−La3, β = Mo−La1−La2, ω = La2−La3−La4, γ = La3−La4−La6, θ = La1−La5−La6 and ϕ = Mo−La5−La6,
- four cation−cation distances: La1−La3, La2−La4, and Mo−Mo represent the three "diagonals" of the cage, and Mo−La3 represents the "bottleneck" of tunnels.

Such a cage in β-$La_{1.85}Ba_{0.15}Mo_2O_{8.925}$ is isolated in Figure 4a. The evolutions of these intertetrahedral edge angles and cation−cation distances as a function of temperature have been determined from the data reported in Table 1 and are displayed in Figure 4b. To identify the change in cage geometry at the origin of the larger expansion in nonoccupied cell volume observed at high temperature for β-$La_{1.85}Ba_{0.15}Mo_2O_{8.925}$, the temperature dependences of the above geometrical parameters were compared with those obtained for β-$La_{1.7}Bi_{0.3}Mo_2O_9$. As observed for the Bi-substituted $La_2Mo_2O_9$, two different thermal behaviors of the tilt angle |δ| are noticed for β-$La_{1.85}Ba_{0.15}Mo_2O_{8.925}$. After a steady state in the temperature range from RT to 400 °C, the tilt angle |δ| starts to increase before leveling off at temperatures higher than 600 °C. Note that the leveling off in β-$La_{1.85}Ba_{0.15}Mo_2O_{8.925}$ occurs at a temperature lower than that observed for β-$La_{1.7}Bi_{0.3}Mo_2O_9$ (∼800 °C), thus softening up the rise of antitetrahedra tilting in the Ba-substituted LAMOX over the temperature range of 400−900 °C. In β-$La_{1.85}Ba_{0.15}Mo_2O_{8.925}$, this increase of the tilt angle |δ| is, in regard to magnitude ($\Delta|\delta_{400-900\ °C}| \approx 0.8°$), almost two times smaller than that observed for β-

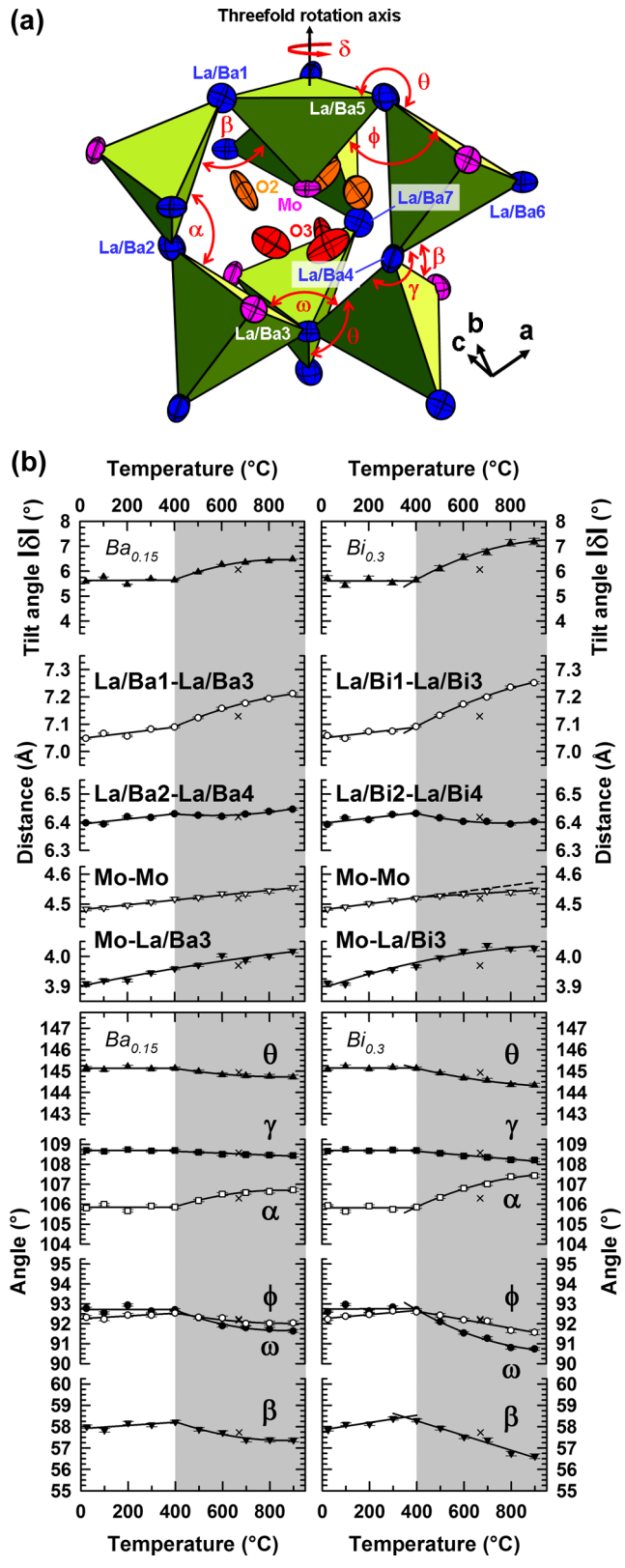

Figure 4. (a) Cage of the three-dimensional (3D) cationic framework, built up from seven La/Ba corner-sharing $[O1(La/Ba)_3Mo]$ antitetrahedral basic units (green) hosting mobile O2/O3 oxide ions in β-$La_{1.85}Ba_{0.15}Mo_2O_{8.925}$. Thermal ellipsoids (at 50% probability) of Mo^{6+} (pink), La^{3+} or Ba^{2+} (blue), O2 (orange), and O3 (red) ion sites determined at room temperature from Rietveld refinement of neutron diffraction data (Table 1). (b) Comparison of temperature dependences of cation–cation distances and intertetrahedral edge angles within the cage for β-$La_{1.85}Ba_{0.15}Mo_2O_{8.925}$ (left) with that for β-$La_{1.7}Bi_{0.3}Mo_2O_9$ (right, ref 26). Variations are satisfactorily fitted with quadratic polynomial functions when departure from steady state or linear behavior is observed. The values determined for β-$La_2Mo_2O_9$ at 670 °C (crosses) are added for reference (see details in the text).

$La_{1.7}Bi_{0.3}Mo_2O_9$ ($\Delta|\delta_{400-900\ °C}| \approx 1.5°$). Nevertheless, Figure 4b shows that edge angles and cation–cation distances within the cage of Ba-substituted LAMOX compound behave the same way as in β-$La_{1.7}Bi_{0.3}Mo_2O_9$ when the tilt angle $|\delta|$ increases in the range of 400–900 °C. Even if the magnitude of the opening or closing of the intertetrahedral edge angles α ($\Delta\alpha \approx +0.9°$), γ ($\Delta\gamma \approx -0.2°$), θ ($\Delta\theta \approx -0.4°$), ϕ ($\Delta\phi \approx -0.5°$), β ($\Delta\beta \approx -0.8°$), and ω ($\Delta\omega \approx -1.1°$) in β-$La_{1.85}Ba_{0.15}Mo_2O_{8.925}$ is nearly twice as small as that observed for β-$La_{1.7}Bi_{0.3}Mo_2O_9$ ($\Delta\alpha \approx +1.6°$, $\Delta\gamma \approx -0.5°$, $\Delta\theta \approx -0.8°$, $\Delta\phi \approx -1°$, $\Delta\beta \approx -1.3°$, and $\Delta\omega \approx -2°$), a closing down of framework's tunnels also occurs in the Ba-substituted LAMOX compound. Theses comparable evolutions tend to suggest that the observed thermal behavior is characteristic of La-substituted β-LAMOX compounds.

Let us now examine how the geometry of the $[O1(La/Ba)_3Mo]$ elementary building unit evolves with temperature. Figure 5 displays the thermal evolution of the La/Ba–La/Ba

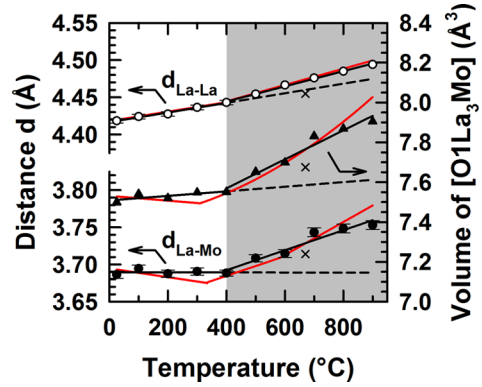

Figure 5. Comparison of thermal evolution of La–La and La–Mo edge lengths (Å) and of the volume (Å^3) of the $[O1La_3Mo]$ antitetrahedral basic unit in $La_{1.85}Ba_{0.15}Mo_2O_{8.925}$ (open/black circles and black triangles) with that in β-$La_{1.7}Bi_{0.3}Mo_2O_9$ (solid red line, see ref 26). The values determined for β-$La_2Mo_2O_9$ at 670 °C (cross symbols, ×) are added for reference (see details in the text).

and La/Ba–Mo distances within the $[O1(La/Ba)_3Mo]$ basic unit, determined from the experimental data reported in Table 1. Below and above 400 °C, La/Ba–La/Ba edges undergo two linear regimes of elongation (see Figure 5). The rates of lengthening ($\Delta d_{La/Ba-La/Ba}/\Delta T \approx 6.5 \times 10^{-5}$ Å °C^{-1} and $\Delta d_{La/Ba-La/Ba}/\Delta T \approx 10.2 \times 10^{-5}$ Å °C^{-1} in the temperature ranges of RT–400 °C and 400–900 °C, respectively) are comparable to those determined for La/Bi–La/Bi edges in the Bi-substituted $La_2Mo_2O_9$ sample ($\Delta d_{La/Bi-La/Bi}/\Delta T \approx 6.2 \times 10^{-5}$ Å °C^{-1} and $\Delta d_{La/Bi-La/Bi}/\Delta T \approx 10.8 \times 10^{-5}$ Å °C^{-1} in the temperature ranges of RT–400 °C and 400–900 °C, respectively). When the temperature increases from RT to 400 °C for β-$La_{1.85}Ba_{0.15}Mo_2O_{8.925}$, the La–Mo edges do not exhibit the slight contraction in length that is observed in Bi-substituted $La_2Mo_2O_9$, their lengths remaining constant up to 400 °C. Above 400 °C, an elongation of the La/Ba–Mo edges

($\Delta d_{La/Ba-Mo}/\Delta T \approx 12.9 \times 10^{-5}$ Å °C^{-1}) takes place, which is of lesser magnitude than the elongation of La/Bi−Mo edges determined in β-$La_{1.7}Bi_{0.3}Mo_2O_9$ ($\Delta d_{La/Ba-Mo}/\Delta T \approx 18.6 \times 10^{-5}$ Å °C^{-1}). It implies that the volume of the antitetrahedron in the barium derivative does not expand as much as that in β-$La_{1.7}Bi_{0.3}Mo_2O_9$ over the range of 400−900 °C (see Figure 5, reduction of the expansion by approximately −0.11 Å^3 at 900 °C). Thus, when the mean La-site cation radius slightly increases by $\Delta\langle r\rangle$ = +0.013 Å, the volume of the cationic framework, which is the cumulative volume of the four antitetrahedra contained in the unit cell, contracts by approximately (−0.11 × 4) Å^3 at 900 °C.

Our previous thorough structural analysis, carried out on the Bi-substituted LAMOX, suggested that, above 400 °C, the distortion/libration of the cationic tetrahedral [$(La/Bi)_3Mo$] coordination of O1 oxide ion allows it to pass through the [$(La/Bi)_3$] and [$(La/Bi)_2Mo$] triangular faces toward nearest-neighboring vacancies at O2 or O3 sites. A structural evidence for the participation of site O1 to the oxide ion migration process above 400 °C in β-$La_{1.7}Bi_{0.3}Mo_2O_9$, was that O1 atom progressively moved away from the [La_3] base of the [$O1(La/Bi)_3Mo$] antitetrahedron as the trigonal extension of this entity along the Mo apex increases in magnitude upon heating above this temperature (increase of the O1−La/Bi and O1−Mo distances). As shown in Figure S1 in the Supporting Information, and ref 26, O1−La/Ba and O1−Mo bond lengths in β-$La_{1.85}Ba_{0.15}Mo_2O_{8.925}$ behave, in the temperature range of 400−900 °C, the same way as in β-$La_{1.7}Bi_{0.3}Mo_2O_9$. What we examine next is whether the increase of the mean La-site cation radius allows the O1 oxide ion to pass through the [La_3] and [$(La)_2Mo$] triangular faces more easily or less easily. The radius r of the sphere tangent to the three atoms forming a triangular face of the antitetrahedron was calculated at each temperature for the two face types [$(La/Ba)_2Mo$] and [$(La/Ba)_3$], according to the method detailed in ref 26. The temperature dependences of r for both [$(La/Ba)_2Mo$] and [$(La/Ba)_3$] triangles and of the equivalent isotropic temperature factors for La/Ba and Mo atoms are shown in Figure 6. In this figure, one can note that the two types of bottlenecks in β-$La_{1.85}Ba_{0.15}Mo_2O_{8.925}$ are slightly narrower than those existing in the Bi compound (difference in size varying from 0.01 to 0.02 Å). Even if a reduction in the size of the bottlenecks was expected, because of the contraction in volume of the antitetrahedron, one can note that this reduction is, however, of the same order of magnitude as the increase of the mean La-site cation radius ($\Delta\langle r\rangle$ = +0.013 Å). When compared to the ionic radius r_O = 1.36 Å[29] of an oxide ion in triangular coordination, the size of the two bottlenecks are too narrow in both compounds for an oxide ion to pass through the faces of the antitetrahedron, regardless of the temperature considered. In β-$La_{1.7}Bi_{0.3}Mo_2O_9$, it has been shown that, above 400 °C, the extra increase of thermal vibrations for La/Bi and Mo atoms favors the distortion/opening of the bottlenecks, allowing the O1 ion migration. Comparing the strength of the Ba−O bond (562.0(13.4) kJ/mol[42]) with that of the Bi−O bond (337.2(13.6) kJ/mol[42]) and considering the large Debye−Waller thermal factor of oxygen atoms, one would expect that the vibration of the Ba atom would be of much higher magnitude than the vibration of the heavier Bi atom. In Figure 6, surprisingly, the reverse situation is observed. At 900 °C, a huge difference of 2 Å^2 is even noted between the atomic displacement parameters for La/Bi and La/Ba atoms. Over the range 400−900 °C, the atomic displacement parameter for Mo

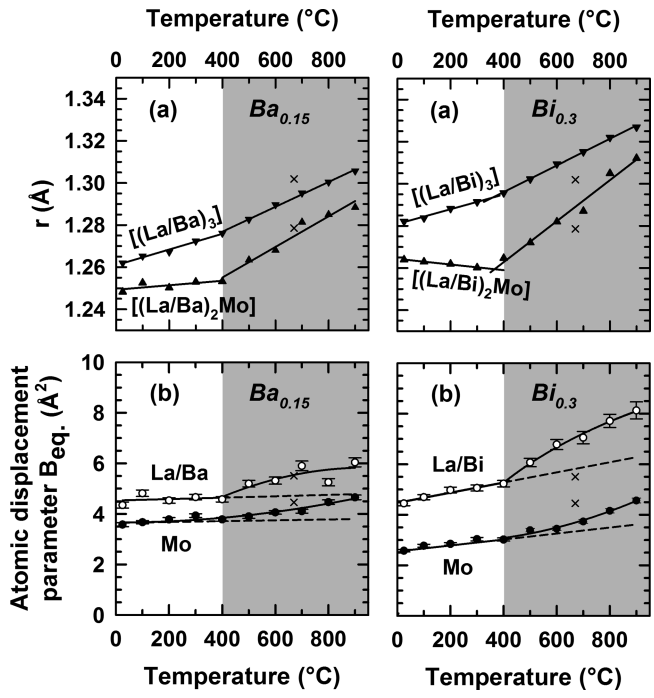

Figure 6. (a) Comparison of temperature dependences of the radius r of the sphere tangent to the three atoms forming a triangular face of the [$O1La_3Mo$] antitetrahedron in β-$La_{1.85}Ba_{0.15}Mo_2O_{8.925}$ (left) with that in β-$La_{1.7}Bi_{0.3}Mo_2O_9$ (right, ref 26). (b) Comparison of temperature dependences of equivalent isotropic temperature factors B_{eq} for La and Mo atoms in β-$La_{1.85}Ba_{0.15}Mo_2O_{8.925}$ (left) and β-$La_{1.7}Bi_{0.3}Mo_2O_9$ (right, ref 26). In panels (a) and (b), the values for β-$La_2Mo_2O_9$ at 670 °C (cross symbols, ×) are added for reference (see details in the text).

atom in the Ba-substituted compound does not increase as much as that in β-$La_{1.7}Bi_{0.3}Mo_2O_9$, since it was already higher in the former than in the latter at temperatures below 400 °C (a difference of ∼1 Å^2). Despite this, both compounds have the same atomic displacement parameter for Mo atom at 900 °C. From this consideration, the jumps of O1 oxygen ions toward the nearest-neighboring O2 and O3 sites in β-$La_{1.85}Ba_{0.15}Mo_2O_{8.925}$ seems to be less assisted by La/Ba atoms than by La/Bi atoms in the Bi-substituted compound. Nevertheless, the conductivity of both compounds remains similar above 450 °C.

This contradiction incited us to closely look into the thermal evolution of the volumes of the cage and tunnels hosting mobile O2 and O3 ions in both compounds. The cage volume can be roughly estimated from the volume of the trigonal bipyramid centered on O3 sites and formed by Mo, La2, La3, La4, and La7 atoms, as shown in Figure 4a (calculation details are given in ref 26). The volume of tunnels is calculated by subtracting the volume of the framework from the volume of the cubic unit cell. The volume variations of the cage and of tunnels against temperature are displayed in Figure 7 for both β-$La_{1.85}Ba_{0.15}Mo_2O_{8.925}$ and β-$La_{1.7}Bi_{0.3}Mo_2O_9$ oxides. In the Ba-substituted compound, the volume of the cage undergoes two successive linear regimes of expansion below and above 400 °C (Figure 7a). Over the range of RT−400 °C, the expansion of the cage in the Bi-substituted compound (∼0.61 Å^3) is slightly higher than in β-$La_{1.85}Ba_{0.15}Mo_2O_{8.925}$ (∼0.53 Å^3). The difference mainly arises from the compression of the antitetrahedron along the [O1−Mo] direction taking place

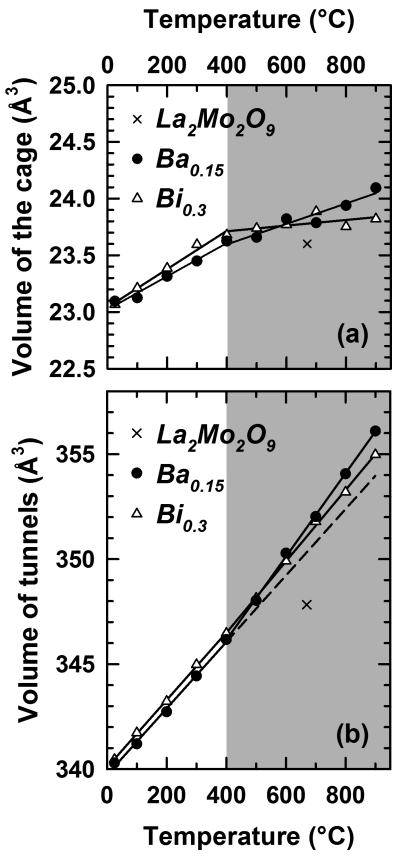

Figure 7. Volume variations of (a) the cage and (b) the tunnels of the 3D cationic framework, as a function of temperature in β-$La_{1.85}Ba_{0.15}Mo_2O_{8.925}$ (black circles, ●) and in β-$La_{1.7}Bi_{0.3}Mo_2O_9$ (open triangles, △, ref 26). The values determined for β-$La_2Mo_2O_9$ at 670 °C (cross symbols, ×) are added for reference (see details in the text).

only in β-$La_{1.7}Bi_{0.3}Mo_2O_9$, which releases extra space in the cage. In the Ba derivative of $La_2Mo_2O_9$, the expansion of the cage at temperatures lower than 400 °C is only due to the elongation of La/Ba1−La/Ba3 and La/Ba2−La/Ba4 distances as the temperature increases (see Figure 4b). Above 400 °C, a slowing of the cage expansion is observed in β-$La_{1.85}Ba_{0.15}Mo_2O_{8.925}$, because of the trigonal extension of the antitetrahedron along the nonbridging Mo apex when it tilts in the cage. Over the range of 400−900 °C, the higher extension and the twice-higher tilting in the cage of the antitetrahedron in β-$La_{1.7}Bi_{0.3}Mo_2O_9$ change the slowing of the cage expansion observed in β-$La_{1.85}Ba_{0.15}Mo_2O_{8.925}$ into a leveling off in the former. Thereby, the volume expansion of the cage in β-$La_{1.85}Ba_{0.15}Mo_2O_{8.925}$ (∼0.47 Å^3) over the range of 400−900 °C is three times higher than that reported in the Bi-substituted compound (∼0.14 Å^3). For all that, the cage in the Ba-substituted compound exceeds in volume the cage in β-$La_{1.7}Bi_{0.3}Mo_2O_9$ above 600 °C only, with the difference in volume at 900 °C attaining a value of ∼0.27 Å^3. Note that this volume expansion of the cage at 900 °C does not correspond in magnitude to the volume contraction of the antitetrahedral framework reported at the same temperature (∼−0.44 Å^3) when the mean La-site cation radius increases. The remaining volume released by this contraction (∼0.17 Å^3) is then inevitably distributed in the intercage space within the tunnels. In Figure 7b, one can however notice that the expansion of tunnels due to the contraction of the antitetrahedra (∼0.44 Å^3) represents only 38.9% of the entire volume expansion of tunnels (∼1.13 Å^3) reported at 900 °C when the mean La-site cation radius increases. It points out that most of the volume expansion of tunnels above 400 °C arises from a decrease of the antitetrahedra tilting caused by the increase in size of the ion bridging three entities. As a matter of fact, a difference in behavior is noticed when comparing the volume expansion of tunnels as a function of temperature in both compounds (see Figure 7b). Whereas the volume of tunnels in β-$La_{1.7}Bi_{0.3}Mo_2O_9$ continues to increase linearly above 400 °C with the same expansion rate that at low temperature, the tunnels in β-$La_{1.85}Ba_{0.15}Mo_2O_{8.925}$ exhibit, above 400 °C, an extra volume expansion, relative to its regular expansion observed at lower temperature. The release of extra empty space in the tunnels of the antistructure above 400 °C could make the migration of O2 and O3 ions within the tunnels easier in the barium derivative than in the bismuth one. Nevertheless, the conductivity of β-$La_{1.85}Ba_{0.15}Mo_2O_{8.925}$ and β-$La_{1.7}Bi_{0.3}Mo_2O_9$ remains similar within the framework-assisted migration regime (see Figure 1 and the conductivity curve reported by Marrero-López et al.[6]). It suggests that, in the barium derivative of β-$La_2Mo_2O_9$, either the easier migration of oxide ions in the tunnels balance the lower ability for O1 ion to escape its tetrahedral surrounding (and *vice versa* in the bismuth derivative) or this extra empty space is not available for migration. To be firmly conclusive about this point, attempts to determine the "free" volume and its role in the oxide ion conduction for both studied samples are presented in the next section.

On the Relative Role of "Free" Volume in the Oxide Ion Conduction. When a departure from linearity is observed at temperatures higher than 450 °C in β-$La_{1.85}Ba_{0.15}Mo_2O_{8.925}$ and 480 °C in β-$La_{1.7}Bi_{0.3}Mo_2O_9$, the temperature dependence of the conductivity can be satisfactorily fitted with the empirical VTF model,

$$\sigma T = \sigma_0 \exp\left[- \frac{B}{R(T - T_0)} \right]$$

as reflected in the high correlation coefficients r^2 obtained, respectively (see Figure S2 and Table S1 in the Supporting Information). The values of the pre-exponential factor (σ_0), the pseudo-activation energy (B), and the temperature T_0 are reported for both compounds in Table S1 in the Supporting Information. In their microscopic interpretation of the empirical VTF equation modeling, the molecular transport in a liquid (or temperature dependence of its fluidity) above the glass transition, Cohen and Turnbull[28] assumed that a local "free" volume starts to appear around each molecule in the viscous liquid only above a critical temperature T_0. In their approach, a molecule is pictured as vibrating about an equilibrium position until a redistribution of local "free" volumes opens up, in its vicinity, a void of sufficient size into which it can jump. This redistribution would originate from the libration of the first nearest molecules surrounding the molecule in motion. If a "free volume"-type mechanism drives the oxide anion migration above 400−450 °C in chemically β-stabilized LAMOX compound, it implies that (i) a distribution of local "free" volumes exists only above T_0 within the [La_3Mo] antitetrahedra-based framework hosting mobile oxide ions and (ii) the vibration/distortion of the cationic framework allows a redistribution of local "free" volumes as the oxide ion migrate,

thus facilitating rapid diffusion and reducing the energy barriers along migration pathways.

Below and above 400 °C, the nonoccupied cell volume undergoes two linear regimes of expansion, with the rate of expansion in the range of 400−900 °C being much larger than that at low temperature (see Figure 3). One can consider the thermal expansion of the nonoccupied volume below 400 °C as regular, since it only originates from linear elongations of interatomic distances without any modification in intertetrahedral edge angles θ, γ, α, and ω (see Figure 4). When this regular thermal expansion of the nonoccupied volume observed below 400 °C is extended to higher temperature, a nonoccupied volume in excess (area in red color, Figure 3) is defined. From the above structural analysis, this extra empty volume corresponds to the volume freed by the distortive expansion of the cationic framework taking place above 400 °C (rotation and distortion of the antitetrahedron). A first reasonable guess would be to think that this volume released represents the total "free" volume favoring/increasing the mobility of oxide ions above 400 °C, as defined by Cohen and Turnbull[28] in their microscopic interpretation of the empirical VTF model. In their theory, these authors have quantitatively linked the thermal expansion of the total "free" volume (V_F) to the parameters B and T_0 of the VTF equation:

$$\frac{B}{R(T - T_0)} = \frac{V_F^*}{V_F} \quad (1)$$

where V_F^* is the smallest "free" volume necessary for a jump to occur. In the structure of β-$La_2Mo_2O_9$, the shortest hopping distance is the distance between two neighboring and partially occupied O2 and O3 crystallographic sites. This volume V_F^* is then calculated by subtracting the volume of an oxygen ion (r_O = 1.36 Å[29] in triangular coordination in the structure of β-$La_2Mo_2O_9$[41]) from the volume of the circular cylinder connecting two neighboring O2 and O3 crystallographic sites. Since the "free" volume V_F only starts to appear above a critical temperature T_0, the quantity V_F^* must be calculated at T_0. From the linear evolution of V_F as a function of temperature, deduced from neutron diffraction data and displayed in Figure 3, the intersection with temperature axis gives a critical temperature T_0 very close to 400 °C for both compounds. For each compound, the average O2−O3 distance at 400 °C (calculated from crystallographic data reported in Table 1) is therefore used to define the height of this circular cylinder, allowing one to calculate the volume V_F^*. The temperature dependence of V_F/V_F^* is displayed in Figure 8 for both compounds. From eq 1, the larger the expansion of the "free" volume V_F, the lower the value of the B factor. As expected from the above structural analysis, the magnitude of the "free" volume expansion is higher in β-$La_{1.85}Ba_{0.15}Mo_2O_{8.925}$ than in β-$La_{1.7}Bi_{0.3}Mo_2O_9$. Thereby, the value of the B factor, deduced from the fit of the conductivity curve, should be lower for β-$La_{1.85}Ba_{0.15}Mo_2O_{8.925}$ than that for the Bi-substituted compound. As shown in Table S1 in the Supporting Information, the reverse situation is observed. This discrepancy might mean that the entire nonoccupied volume in excess (the red area delineated in Figure 3) does not correspond to the total "free" volume available for the migration. At this stage, a question can be raised: What is the fraction of nonoccupied volume used for the oxide ion migration in LAMOX materials? Let us now calculate, by using eq 1, the temperature dependence of the total "free" volume from the values of the B factor, and the temperature T_0

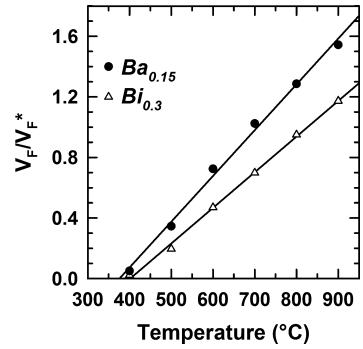

Figure 8. Temperature dependence of V_F/V_F^* for β-$La_{1.85}Ba_{0.15}Mo_2O_{8.925}$ (black circles) and β-$La_{1.7}Bi_{0.3}Mo_2O_9$ (open triangles). V_F and V_F^* are the total "free" volume released above 400 °C by the distortive expansion of the cationic framework and the smallest "free" volume necessary for a jump to occur, respectively.

reported in Table S1 in the Supporting Information, assuming that the value of the volume V_F^* determined previously from the average O2−O3 distance at 400 °C is correct. Figure S3 in the Supporting Information displays the comparison of the temperature dependences of the total "free" cell volumes V_F deduced from the analysis of neutron diffraction patterns and of complex impedance spectra for β-$La_{1.85}Ba_{0.15}Mo_2O_{8.925}$ and β-$La_{1.7}Bi_{0.3}Mo_2O_9$ compounds. In this figure, very low values of V_F are obtained from complex impedance data of both compounds. It would suggest that only a very small fraction of the volume freed by the distortive expansion of the cationic framework (at 900 °C, 6.9% for β-$La_{1.85}Ba_{0.15}Mo_2O_{8.925}$ and 13.3% for β-$La_{1.7}Bi_{0.3}Mo_2O_9$) is really used in the conduction process, which is hard to believe.

Dienes,[30] and Macedo and Litovitz,[31] have tried to reconcile all the existing theories in the field of the modeling of molecular transport in a liquid above the glass transition. In their approach, the molecule can jump into the void resulting from the redistribution of local "free" volumes only if this molecule attains a sufficient energy to overcome the attractive forces holding it to its immediate neighbors. A new equation results from their investigation, which can be seen as a modified version of the VTF equation. The relative effects of "free" volume and intermolecular forces on the transport properties of a liquid are dissociated from one to the other in the Dienes−Macedo−Litovitz (DML) equation.[30,31] In addition to the exponential term $\exp\{-B/[R(T - T_0)]\}$ describing the "free volume" mechanism, a second exponential one that contains an activation energy is introduced in the DML equation. Whereas the "free volume" approach of Cohen and Turnbull failed to describe the temperature dependence of the fluidity of several liquids when the glass-transition temperature (T_g) is exceeded by 100 °C, satisfactory fits with the DML equation were obtained. Most interestingly, this study clearly demonstrated that the "free" volume V_F involved in the transport process is considerably larger than the one predicted by the Cohen and Turnbull theory. As illustrated in the Figure S3 in the Supporting Information, an underestimation of V_F is suspected when fits of the conductivity data with the VTF equation are performed for LAMOX materials. This motivated us to attempt a fit with the empirical DML model when a departure from linearity is observed in the temperature dependence of the conductivity at temperatures higher than 425−450 °C. In a ionic conductor, the activation energy is linked to the formation enthalpy of defects ΔH_f. In a β-$La_2Mo_2O_9$-type oxide ion

conductor, these defects are very likely anion Frenkel pairs $O_O^{\times} \leftrightarrow O_i'' + V_O^{\bullet\bullet}$ in the Kröger−Vink notation.[43] When transposed to the ionic transport in a solid, the DML equation for the fluidity of a liquid becomes:

$$\sigma T = \sigma_0 \exp\left(-\frac{\Delta H_f}{2RT}\right) \exp\left[-\frac{B}{R(T - T_0)}\right] \quad (2)$$

As pointed by Macedo and Litovitz,[31] the data can be obviously fitted with four adjustable parameters (σ_0, ΔH_f, B, and T_0) better than with three (σ_0, B, and T_0). More recently, this equation was used to model the diffusion of alkaline ions in amorphous silicates above the glass-transition temperature (T_g).[44]

In order to restrict the number of parameters refined simultaneously when fitting the conductivity data of a given compound with the DML equation, the values of the pseudo-activation energy B and the temperature T_0 were first determined from the linear regression analysis of the temperature dependence of V_F/V_F^* obtained from neutron diffraction data. For each compound, the two remaining adjustable parameters of the model (pre-exponential factor σ_0 and the formation enthalpy of anion Frenkel pairs ΔH_f) were then refined in a second step when fitting the conductivity curve with the DML equation using the values of B and T_0 parameters determined beforehand. The main advantage of the above procedure lies in the fact that the four parameters are determined through fits of experimental data and never empirically estimated or extrapolated for a part of them (as in ref 44, for instance). It is also a way to possibly reconcile the analyses of neutron diffraction patterns and of complex impedance spectra. As demonstrated in Figure 1 and confirmed by the high value of the correlation coefficient r^2, the temperature dependence of the conductivity for both compounds can be satisfactorily fitted with a DML equation using the set of parameters displayed in Table 2. It is worth noting that the "free volume" term mostly determines the way the conductivity deviates above 400−450 °C from the linear Arrhenius regime at lower temperatures ("bending" term), while the magnitude of the conductivity change is controlled by the "enthalpic" term. From the values tabulated for β-$La_{1.7}Bi_{0.3}Mo_2O_9$ and β-$La_{1.85}Ba_{0.15}Mo_2O_{8.925}$ compounds, the formation enthalpy of the Frenkel defects seems to play a significant role in determining the conductivity above 400−450 °C.

In β-$La_{1.7}Bi_{0.3}Mo_2O_9$, the formation enthalpy of the Frenkel defects (ΔH_f = 1.1 eV) is slightly higher than the value of 0.84 eV found in the literature[45] for the $Ba_2In_2O_5$, which is a brownmillerite oxide ion conductor that has intrinsic oxygen vacancies as $La_2Mo_2O_9$. One can notice that this enthalpy (ΔH_f) significantly increases when the mean La-site ionic radius increases in the β-$La_2Mo_2O_9$ structure. This explains why, despite a higher "free" volume expansion, the ionic conductivity of the β-$La_{1.85}Ba_{0.15}Mo_2O_{8.925}$ compound above 450 °C remains similar to that of the bismuth compound. A question immediately arises: Why is the formation enthalpy of the Frenkel defects (ΔH_f) in β-$La_{1.85}Ba_{0.15}Mo_2O_{8.925}$ so high? Atomistic simulation or density functional theory (DFT) calculations[46,47] and EXAFS/XANES[48] measurements carried on yttria-stabilized zirconia reveal that the Y^{3+} cation, which is larger in size than the host Zr^{4+} cation, is preferentially located in the second-nearest-neighbor position with respect to the oxygen vacancy, thus implying that the vacancy is the first nearest neighbor to the host Zr^{4+} cation. This result is consistent with ^{89}Y NMR study of 8 mol % yttria-stabilized zirconia, showing that 95% and 5% of Y ions are 8-fold and 7-fold coordinated, respectively, to oxygen in the cubic fluorite-type structure.[49] When the size of the substitute is very close to that of the host Zr^{4+} cation (the Sc^{3+} cation, for instance), a random vacancy distribution is achieved. It explains why Sc_2O_3-stabilized zirconia has the highest conductivity and the lowest activation energy of any known single aliovalently substituted zirconia.[47,50] Taking into account the large size mismatch existing between La^{3+} and Ba^{2+} ions (difference in size of 0.25 Å with ionic radius in 10-fold coordination[29]), one can assume that the oxygen vacancies $V_O^{\bullet\bullet}$ in β-$La_{1.85}Ba_{0.15}Mo_2O_{8.925}$ are preferentially located/formed in the surroundings of the La ion rather than that of the larger Ba^{2+} cation. When barium replaces lanthanum in the first-nearest-neighbor sphere of an oxide ion residing in a crystallographic site $O_O^{\times}$, it would become less energetically favorable for this oxide ion to jump into an interstitial site O_i'' and create an oxygen vacancy $V_O^{\bullet\bullet}$ in place of the original oxygen site. Thus, it gives a plausible explanation of the high enthalpy ΔH_f determined for β-$La_{1.85}Ba_{0.15}Mo_2O_{8.925}$. The fact that the β-$La_{1.7}Bi_{0.3}Mo_2O_9$ sample, for which the size mismatch between the host La^{3+} cation and the substitute (difference in size of 0.04 Å for the La^{3+}/Bi^{3+} pair with the ionic radius in 10-fold coordination[29]) is the smallest, is also the composition having the lowest formation enthalpy of anion Frenkel $O_i'' + V_O^{\bullet\bullet}$ pairs (see Table 2) strengthens this explanation. However, no certainty on a full random distribution of oxygen vacancies in β-$La_{1.7}Bi_{0.3}Mo_2O_9$ can be claimed from this single criterion of size. Experimental evidence is needed to be firmly conclusive about this point. It is reasonable to think that the decrease of the conductivity observed in all cubic-substituted LAMOX compounds, chemically stabilized by K^+ or Pb^{2+} cations larger than La^{3+} in size,[6,8] would also partially originate from the uneven distribution of oxygen vacancies in the structure.

Identify a Substitution Strategy To Enhance the Oxide Ion Conduction of Chemically β-Stabilized LAMOX Compounds. Given what we observed for β-$La_{1.85}Ba_{0.15}Mo_2O_{8.925}$ and β-$La_{1.7}Bi_{0.3}Mo_2O_9$ samples, the substitution strategy of La to enhance the oxide ion conduction in chemically β-stabilized LAMOX compounds could be to optimize both the size match between lanthanum and the substituting element and the "free" volume expansion. If we consider the size match in β-$La_2Mo_2O_9$ as ideal, what is the ideal "free" volume in this binary oxide? However, the "free" volume expansion resulting from the progressive rotation and distortion of the antitetrahedra in β-$La_2Mo_2O_9$ cannot be determined, because of the first-order nature of its α/β structural phase transition at 580 °C. Our attention was then focused on the nonoccupied cell volume, which is much easier to calculate. In addition, all structural parameters (tilting angle, volume of the antitetrahedron, size of the bottlenecks, etc.) analyzed in the present study were also determined for the parent compound $La_2Mo_2O_9$ from neutron diffraction data collected at 670 °C (above its structural α/β phase transition). The crystal structure of β-$La_2Mo_2O_9$ at 670 °C (see the CIF file in the Supporting Information) has been refined by the Rietveld method constraining the occupancy of the O3 site with that of the O2 site, as previously done for β-$La_{1.85}Ba_{0.15}Mo_2O_{8.925}$ and β-$La_{1.7}Bi_{0.3}Mo_2O_9$ compounds. Once the structural parameters for $La_2Mo_2O_9$ were determined from these crystallographic data, they were compared with those

obtained for the Ba- and Bi-substituted compounds (cross symbol (×) in Figures 3−7).

First of all, the unit-cell volume of β-$La_2Mo_2O_9$ (V = 378.53(2) Å^3) at 670 °C is determined to be smaller than the volumes calculated at this temperature for β-$La_{1.85}Ba_{0.15}Mo_2O_{8.925}$ (V = 382.60 Å^3) and β-$La_{1.7}Bi_{0.3}Mo_2O_9$ (V = 382.20 Å^3) from a linear regression. But, most interestingly, the volume variation of the unit cell is 15 or 7 times higher in magnitude than the gain (∼0.26 Å^3) or the loss (∼−0.50 Å^3) of nonoccupied volume solely caused by the partial La/Ba or La/Bi substitution, respectively. In terms of nonoccupied volume, its fraction for β-$La_2Mo_2O_9$ at 670 °C (∼40.4%) remains 0.4%−0.6% smaller than that calculated at this temperature for β-$La_{1.7}Bi_{0.3}Mo_2O_9$ and β-$La_{1.85}Ba_{0.15}Mo_2O_{8.925}$ compounds, respectively (see Figure S4 in the Supporting Information). It is worth mentioning that the tilt angle $|\delta|$ (Figure 4), the volume of the antitetrahedron (Figure 5), and the volume of tunnels (Figure 7) in β-$La_2Mo_2O_9$ at 670 °C are similar to the angle and volumes calculated for the substituted compounds at only 500 °C. However, the conductivity of the two chemically β-stabilized LAMOX compounds at 500 °C ($1000/T \approx 1.29$ K^{-1} in Figure 1) remains much lower than the conductivity measured in the parent compound at 670 °C ($1000/T \approx 1.06$ K^{-1}). It clearly suggests that increasing the fraction of nonoccupied volume (of total "free" volume) in the framework of β-$La_2Mo_2O_9$ through relevant cationic substitution is not a way to enhance its oxide ion conduction. Thereby, the key parameter that determines, or has a strong impact on, the conductivity is the size match between lanthanum and the element substituting for it, rather than a high "free" volume expansion. For all of that, no matter how partial the role of the "free" volume expansion is in determining the conductivity, a minimum expansion is, however, required to ensure the assisted migration of oxide ions above 400−450 °C. Keeping the fraction of nonoccupied volume (or of the "free" volume) above 600 °C in β-stabilized LAMOX as low as it is in β-$La_2Mo_2O_9$ could be a way to reach this minimum expansion of total "free" volume. An example to illustrate this point is the thermodynamically stable β-$La_{1.75}Eu_{0.25}Mo_2O_9$ phase.[13] At 670 °C, the pure and the Eu-substituted compounds have almost the same (minimum) fraction of the nonoccupied volume (∼40.40% and ∼40.35%, respectively, calculated from XRD data[13]). At 670 °C, the ionic conductivity of the β-$La_{1.75}Eu_{0.25}Mo_2O_9$ phase[13] is lower than that measured for β-$La_2Mo_2O_9$. In this Eu-substituted LAMOX compound, a large size mismatch exists between lanthanum and the substitute (mean La site cation radius $\langle r \rangle$ from 1.27 Å to 1.259 Å with an ionic radius for La^{3+} and Eu^{3+} in 10-fold coordination of 1.27 and 1.18 Å, respectively). Because of the very small difference in the fraction of the nonoccupied volume between β-$La_{1.75}Eu_{0.25}Mo_2O_9$ and β-$La_2Mo_2O_9$, the decrease of the conductivity observed when La^{3+} is partially substituted by Eu^{3+} can only be interpreted as originating from the uneven distribution of oxygen vacancies caused by the size mismatch between these two trivalent ions (trapping of oxygen vacancies around Eu^{3+} ions).

4. CONCLUSION

In this paper, the crystal structure of β-$La_{1.85}Ba_{0.15}Mo_2O_{8.925}$ was refined from neutron diffraction data at different temperatures in the range from room temperature (RT) to 900 °C in order to obtain deeper insight into the effect of barium on the transport properties. Whatever the temperature considered, the intrinsic oxygen vacancies, as well as extrinsic ones introduced by the aliovalent substitution of La^{3+} by Ba^{2+}, only reside at the O2 and O3 crystallographic sites, as previously observed in β-$La_{1.7}Bi_{0.3}Mo_2O_9$ or in the parent compound β-$La_2Mo_2O_9$. The antistructure of the cubic Ba-substituted $La_2Mo_2O_9$, built up from La corner-sharing [O1La_3Mo] antitetrahedra, is distorted upon heating the same way as in β-$La_{1.7}Bi_{0.3}Mo_2O_9$. It clearly shows that the complex distortive expansion, previously observed in β-$La_{1.7}Bi_{0.3}Mo_2O_9$, is probably representative of what happens in other La-substituted cubic members of the LAMOX family. When comparing the distortion of the antistructure of the two substituted compounds, the weak increase in the mean La-site cation radius, $\Delta\langle r \rangle$ = +0.013 Å between β-$La_{1.7}Bi_{0.3}Mo_2O_9$ and β-$La_{1.85}Ba_{0.15}Mo_2O_{8.925}$, surprisingly induces a slight decrease in magnitude of the volume expansion of the [O1La_3Mo] antitetrahedron taking place upon heating above 400−450 °C. The resultant small reduction in the size of the triangular [La_3] and [La_2Mo] bottlenecks through which the O1 oxide ion must pass, coupled with the large decrease in vibration amplitude of the La atom, suggest that its migration becomes less easy when the mean La-site ionic radius increases. Concomitantly, in the temperature range of 400−900 °C, the increase in the average size of the ion bridging three [O1La_3Mo] antitetrahedra restricts, in magnitude, the tilting of these entities in the cage and, thereby, the cage distortion. Contrary to what had been earlier observed in β-$La_{1.7}Bi_{0.3}Mo_2O_9$, the tunnels in β-$La_{1.85}Ba_{0.15}Mo_2O_{8.925}$ exhibit, above 400 °C, an extra volume expansion relative to their regular expansion at lower temperature. The release of extra volume in the framework's tunnels results mainly from the weakening of the cage distortion and slightly from the smaller trigonal extension of the antitetrahedron along its nonbridging Mo apex pointing in the cage. This comparative structural study shows that the main structural change caused by barium in the structure concerns the tilt/rotation of the antitetrahedral building units of the cationic framework.

In all derivatives of β-$La_2Mo_2O_9$, a singular increase of the conductivity is observed above 400−450 °C, which can be satisfactorily fitted with the empirical Vogel−Tammann−Fulcher (VTF) model, thus suggesting that the mechanism driving the oxide anion migration is of the "free volume" type. If so, the expansion/distortion of the host cationic framework above 400−450 °C should free up an empty volume favoring the migration of the oxide anion within it, according to the microscopic interpretation of the VTF equation proposed by Cohen and Turnbull. However, the anionic conductivities of β-$La_{1.7}Bi_{0.3}Mo_2O_9$ and β-$La_{1.85}Ba_{0.15}Mo_2O_{8.925}$ remain similar above 400−450 °C, despite a release of extra empty space in the tunnels hosting mobile O2 and O3 ions and the introduction of extrinsic oxygen vacancies in the latter. A deeper analysis of the temperature dependence of the anionic conductivity was performed by using two different models based on/derived from the "free" volume theory of the molecular transport in a liquid. Only the modification of the VTF equation proposed by Dienes, Macedo, and Litovitz allows, for the first time in a crystallized compound, to quantitatively link the singular increase of anionic conductivity above 400−450 °C to the volume expansion of the voids determined from neutron diffraction data. However, most interestingly, this thorough analysis has allowed us to identify the size match between lanthanum and the element substituting for it as a second key parameter that determines the anionic

conductivity in chemically β-stabilized LAMOX compounds. When comparing β-$La_{1.85}Ba_{0.15}Mo_2O_{8.925}$ to the parent compound β-$La_2Mo_2O_9$, it was shown, in this paper, that the size match has a much stronger impact on the conductivity than the "free" volume expansion. This study thus provides a plausible explanation for the conductivity decrease observed by several authors in cubic derivatives of β-$La_2Mo_2O_9$ chemically stabilized by K^+, Ba^{2+}, or Pb^{2+} cations, which are larger in size than La^{3+}. A substitution strategy to enhance the oxide ion conduction of β-stabilized LAMOX compounds, even to reach or exceed that of β-$La_2Mo_2O_9$, would consist of (i) selecting the substitute the closest in size to that of lanthanum in order to promote a random oxygen vacancy distribution in the antistructure and (ii) adjusting the substitute amount to reach the minimum thermal expansion of total "free" volume required to ensure the assisted migration of the oxide ion. To fulfill the second condition, the fraction of nonoccupied volume above 600 °C in β-stabilized LAMOX must be kept as low as it is in β-$La_2Mo_2O_9$. Only a determination of the cubic unit-cell volume of β-stabilized LAMOX compounds through Le Bail fit of the X-ray diffraction (XRD) pattern collected at high temperature is necessary to evaluate this fraction of nonoccupied volume, thus allowing the rapid screening of potential highly conducting compositions.

■ ASSOCIATED CONTENT

Supporting Information

(1) Thermal evolution of O1−cation bond lengths, of the distance between O1 and the $[(La/Ba)_3]$ base and of bond angles within the $[O1(La/Ba)_3Mo]$ antitetrahedral basic unit, as a function of temperature in β-$La_{1.85}Ba_{0.15}Mo_2O_{8.925}$. (2) Dependence of the electrical conductivity at high temperature fitted with the Vogel−Tammann−Fulcher (VTF) model. (3) Comparison of the temperature dependences of the "free" cell volumes (V_F), deduced from the analysis of neutron diffraction patterns and of complex impedance spectra for β-$La_{1.85}Ba_{0.15}Mo_2O_{8.925}$ and β-$La_{1.7}Bi_{0.3}Mo_2O_9$ compounds. (4) Comparison of the fraction of nonoccupied volume in β-$La_{1.7}Bi_{0.3}Mo_2O_9$ and in β-$La_{1.85}Ba_{0.15}Mo_2O_{8.925}$ above 400 °C to that determined in β-$La_2Mo_2O_9$ at 670 °C. (5) Crystallographic data of β-$La_{1.85}Ba_{0.15}Mo_2O_{8.925}$ at RT, 100 °C, 200 °C, 300 °C, 400 °C, 500 °C, 600 °C, 700 °C, 800 °C, and 900 °C in Crystallographic Information File (CIF) format. (6) Crystallographic data of β-$La_2Mo_2O_9$ at 670 °C in Crystallographic Information File (CIF) format.

■ AUTHOR INFORMATION

Corresponding Author

*Tel.: +33 (0)2 43 83 26 48. Fax: +33 (0)2 43 83 35 06. E-mail: gwenael.corbel@univ-lemans.fr.

Notes

The authors declare no competing financial interest.

■ REFERENCES

(1) Lacorre, P.; Goutenoire, F.; Bohnke, O.; Retoux, R.; Laligant, Y. *Nature* **2000**, *404*, 856−858.

(2) Goutenoire, F.; Isnard, O.; Retoux, R.; Lacorre, P. *Chem. Mater.* **2000**, *12*, 2575−2580.

(3) Gibson, I. R.; Irvine, J. T. S. *J. Mater. Chem.* **1996**, *6*, 895−898.

(4) Tealdi, C.; Chiodelli, G.; Malavasi, L.; Flor, G. *J. Mater. Chem.* **2004**, *14*, 3553−3557.

(5) Wang, X. P.; Cheng, Z. J.; Fang, Q. F. *Solid State Ionics* **2005**, *176*, 761−765.

(6) Marrero-Lopez, D.; Perez-Coll, D.; Ruiz-Morales, J. C.; Canales-Vazquez, J.; Martin-Sedeno, M. C.; Nunez, P. *Electrochim. Acta* **2007**, *52*, 5219−5231.

(7) Selmi, A.; Galven, C.; Corbel, G.; Lacorre, P. *Dalton Trans.* **2010**, *39*, 93−102.

(8) Takai, S.; Doi, Y.; Torii, S.; Zhang, J.; Putra, T. Y. S. P.; Miao, P.; Kamiyama, T.; Esaka, T. *Solid State Ionics* **2013**, *238*, 36−43.

(9) Wang, X. P.; Fang, Q. F.; Li, Z. S.; Zhang, G. G.; Yi, Z. G. *Appl. Phys. Lett.* **2002**, *81*, 3434−3436.

(10) Subramania, A.; Saradha, T.; Muzhumathi, S. *J. Power Sources* **2007**, *167*, 319−324.

(11) Marrero-Lopez, D.; Canales-Vazquez, J.; Zhou, W. Z.; Irvine, J. T. S.; Nunez, P. *J. Solid State Chem.* **2006**, *179*, 278−288.

(12) Corbel, G.; Durand, P.; Lacorre, P. *J. Solid State Chem.* **2009**, *182*, 1009−1016.

(13) Corbel, G.; Chevereau, E.; Kodjikian, S.; Lacorre, P. *Inorg. Chem.* **2007**, *46*, 6395−6404.

(14) Marrero-Lopez, D.; Nunez, P.; Abril, M.; Lavin, V.; Rodriguez-Mendoza, U. R.; Rodriguez, V. D. *J. Non-Cryst. Solids* **2004**, *345−46*, 377−381.

(15) Georges, S.; Goutenoire, F.; Altorfer, F.; Sheptyakov, D.; Fauth, F.; Suard, E.; Lacorre, P. *Solid State Ionics* **2003**, *161*, 231−241.

(16) Voronkova, V. I.; Kharitonova, E. P.; Krasil'nikova, A. E. *Crystallogr. Rep.* **2010**, *55*, 276−282.

(17) Basu, S.; Devi, P. S.; Maiti, H. S. *J. Electrochem. Soc.* **2005**, *152*, A2143−A2147.

(18) Khadasheva, Z. S.; Venskovskii, N. U.; Safronenko, M. G.; Mosunov, A. V.; Politova, E. D.; Stefanovich, S. Y. *Inorg. Mater.* **2002**, *38*, 1168−1171.

(19) Mhadhbi, N.; Corbel, G.; Lacorre, P.; Bulou, A. *J. Solid State Chem.* **2012**, *190*, 246−256.

(20) Corbel, G.; Laligant, Y.; Goutenoire, F.; Suard, E.; Lacorre, P. *Chem. Mater.* **2005**, *17*, 4678−4684.

(21) Collado, J. A.; Aranda, M. A. G.; Cabeza, A.; Olivera-Pastor, P.; Bruque, S. *J. Solid State Chem.* **2002**, *167*, 80−85.

(22) Arulraj, A.; Goutenoire, F.; Tabellout, M.; Bohnke, O.; Lacorre, P. *Chem. Mater.* **2002**, *14*, 2492−2498.

(23) Vogel, H. *Phys. Z.* **1921**, *22*, 645−646.

(24) Tammann, G.; Hesse, W. *Z. Anorg. Allg. Chem.* **1926**, *156*, 245−257.

(25) Fulcher, G. S. *J. Am. Ceram. Soc.* **1925**, *8*, 339−355.

(26) Corbel, G.; Suard, E.; Lacorre, P. *Chem. Mater.* **2011**, *23*, 1288−1298.

(27) Lacorre, P.; Selmi, A.; Corbel, G.; Boulard, B. *Inorg. Chem.* **2006**, *45*, 627−635.

(28) Cohen, M. H.; Turnbull, D. *J. Chem. Phys.* **1959**, *31*, 1164−1169.

(29) Shannon, R. D. *Acta Crystallogr., Sect. A: Cryst. Phys., Diffr., Theor.: Gen. Crystallogr.* **1976**, *32*, 751−767.

(30) Dienes, G. J. *J. Appl. Phys.* **1953**, *24*, 779−782.

(31) Macedo, P. B.; Litovitz, T. A. *J. Chem. Phys.* **1965**, *42*, 245−256.

(32) Rodriguez Carvajal, J. *Physica B* **1993**, *192*, 55−69.

(33) Berar, J. F.; Baldinozzi, G. *J. Appl. Crystallogr.* **1993**, *26*, 128−129.

(34) Fender, B. E. F. *Chemical Applications of Thermal Neutron Scattering*; Willis, B. T. M., Ed.; Oxford University Press: London, 1974.

(35) Aldebert, P.; Dianoux, A. J.; Traverse, J. P. *J. Phys. (Paris)* **1979**, *40*, 1005−1012.

(36) Johnson, P. A. V.; Wright, A. C.; Sinclair, R. N. *J. Non-Cryst. Solids* **1983**, *58*, 109−130.

(37) Bergerhoff, G.; Berndt, M.; Brandenburg, K. *J. Res. Natl. Inst. Stand. Technol.* **1996**, *101*, 221−225.

(38) Hamilton, W. C. *Acta Crystallogr.* **1959**, *12*, 609−610.

(39) Brown, I. D.; Dabkowski, A.; McCleary, A. *Acta Crystallogr., Sect. B: Struct. Sci.* **1997**, *53*, 750−761.

(40) Andersson, S.; Åström, A. NBS Special Publication 364, Solid State Chemistry. In *Proceedings of the 5th Material Research Symposium*, 1972; p 3.
(41) Emery, J.; Massiot, D.; Lacorre, P.; Laligant, Y.; Conder, K. *Magn. Reson. Chem.* **2005**, *43*, 366−371.
(42) *CRC Handbook of Chemistry and Physics 2008−2009: A Ready-Reference Book of Chemical and Physical Data*; 89th Edition; Lide, D. R., Ed.; CRC Press: Boca Raton, FL, 2008.
(43) Kröger, F. A.; Vink, H. J. *Solid State Phys.* **1956**, *3*, 307−435.
(44) Souquet, J.-L.; Nascimento, M. L. F.; Rodrigues, A. C. M. *J. Chem. Phys.* **2010**, *132*, 034704.
(45) Zhang, G. B.; Smyth, D. M. *Solid State Ionics* **1995**, *82*, 161−172.
(46) Zacate, M. O.; Minervini, L.; Bradfield, D. J.; Grimes, R. W.; Sickafus, K. E. *Solid State Ionics* **2000**, *128*, 243−254.
(47) Bogicevic, A.; Wolverton, C.; Crosbie, G. M.; Stechel, E. B. *Phys. Rev. B* **2001**, *64*, 014106.
(48) Li, P.; Chen, I. W.; Penner-Hahn, J. E. *Phys. Rev. B* **1993**, *48*, 10074−10081.
(49) Maekawa, H.; Kawata, K.; Xiong, Y. P.; Sakai, N.; Yokokawa, H. *Solid State Ionics* **2009**, *180*, 314−319.
(50) Badwal, S. P. S.; Ciacchi, F. T.; Milosevic, D. *Solid State Ionics* **2000**, *136−137*, 91−99.